Supporting Information

A Self-Growing 3D Porous Sn Protective Layer Enhanced Zn Anode

Dezhi Kong [1], Qingwei Zhang [1], Lin Li [2], Huimin Zhao [1], Ruixin Liu [1], Ziyang Guo [1,*] and Lei Wang [1,3,*]

[1] Key Laboratory of Eco-Chemical Engineering, Taishan Scholar Advantage and Characteristic Discipline Team of Eco-Chemical Process and Technology, College of Chemistry and Molecular Engineering, Qingdao University of Science and Technology, Qingdao 266042, China
[2] School of Materials Science and Engineering, Suzhou University of Science and Technology, Suzhou 215009, China
[3] College of Environment and Safety Engineering, Qingdao University of Science and Technology, Qingdao 266042, China
* Correspondence: zyguo@qust.edu.cn (Z.G.); inorchemwl@qust.edu.cn (L.W.); Tel./Fax: +86-0532-8402-3409 (L.W.)

Characterization instrumentation

X-ray diffraction (XRD) measurements were conducted on a Rigaku-D/MAX/2500 PC instrument (Japan). Scanning electron microscopy (SEM) investigations were examined using the Hitachi Regulus-8100 (Japan). X-ray photoelectron spectroscopy (XPS) was measured via Kratos AXIS SUPRA (UK) using an Al anode as a source with C 1s at 284.6 eV as a reference standard to revise the binding energy and X-ray photoelectron spectroscopy were recovered from all water cells in the CR2032 coin cell configuration.

Electrochemical measurements

To measure the corrosion rate in a 2M $ZnSO_4$ electrolyte, a three-electrode configuration was used with the bare Zn or ZSN electrode as the working electrode, a Pt foil as the counter electrode, and a saturated glymeric electrode as the reference electrode. Linear polarization measurements (CHI760E) were performed at a scan rate of 5 mV s^{-1} from -0.2 to -1.8 V using CHI760E (CH Instruments Ins) on a saturated glycury electrode. The current density was obtained by dividing the measured current by the active surface area of the bare Zn or ZSN electrode. To determine the ionic conductivity, electrochemical impedance spectroscopy of assembled CR2032 cells (same assembly as above) was collected using a CHI760E constant potential meter. The frequency range was from 50,000 to 0.01 with an amplitude of 10 mV. The open circuit potential was set as the initial voltage. The reversibility of zinc stripping/plating was examined by assembled CR2032 button cells using CHI760E cyclic voltammetry from -0.2 to -1.8 V at scan rates from 5 mV s^{-1} to 50 mV s^{-1}. Constant current cycling of symmetrical batteries was performed with the LANHE CT2001 battery test system (LAND Electronics). Pre-activated for 5 cycles at 0.5 ma cm^{-2} and 0.5 mah cm^{-2}. Constant current cycling of Zn‖ MVO full cells and Zn‖ AC supercapacitors using the LANHE CT2001 battery test system (LAND Electronics). The cells were initially discharged to 0.2 V and then charged to 1.8 V at a specific current density.

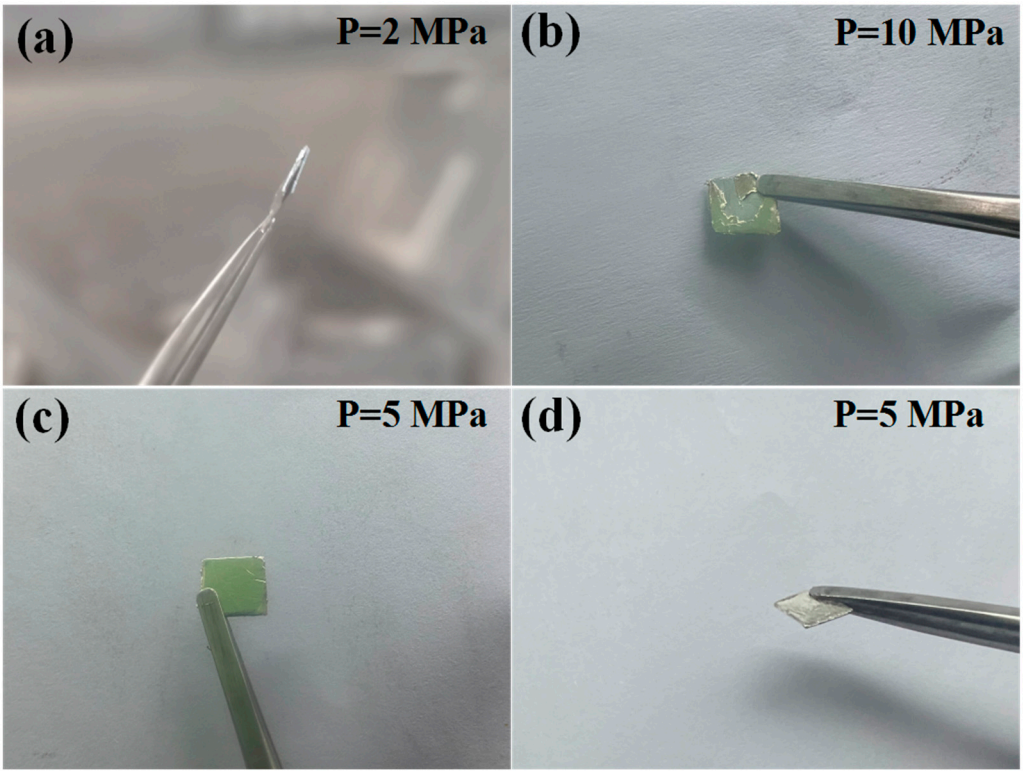

Figure S1. Photos of Zn-Li foil under different pressures: (a) 2 MPa; (b) 10 MPa; and (c,d) 5 MPa.

Figure S2. The thickness of the Zn-Li foil.

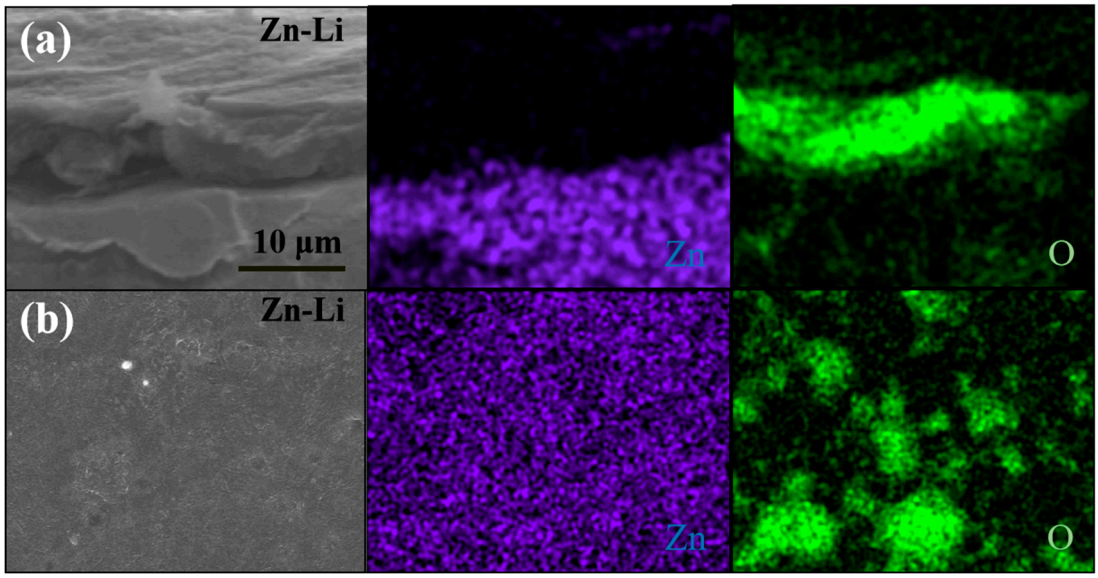

Figure S3. SEM/EDS analysis from the (a) cross section and (b) surface of Zn-Li foil.

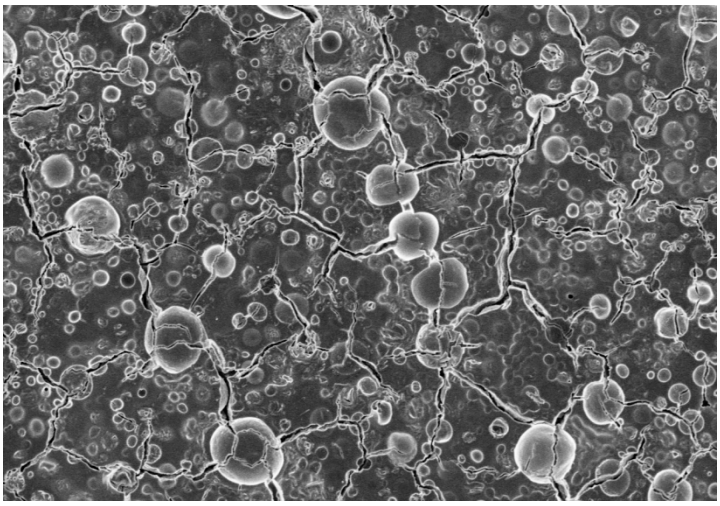

Figure S4. SEM image of the ZS electrode.

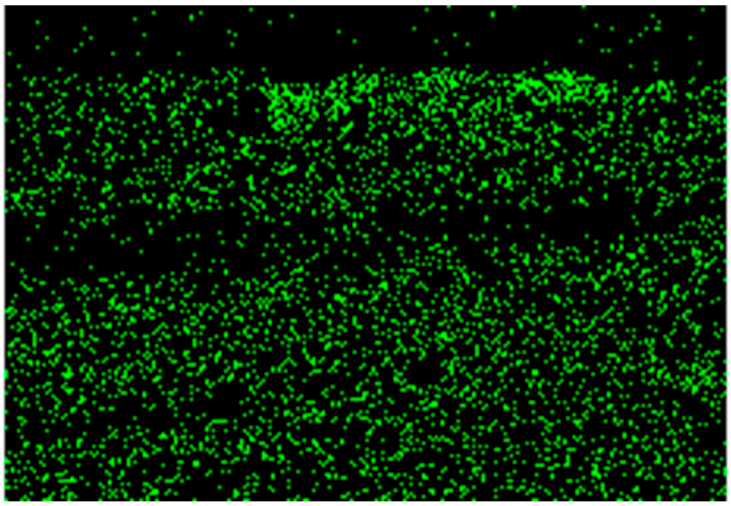

Figure S5. The cross-sectional corresponding EDS element mapping (Sn).

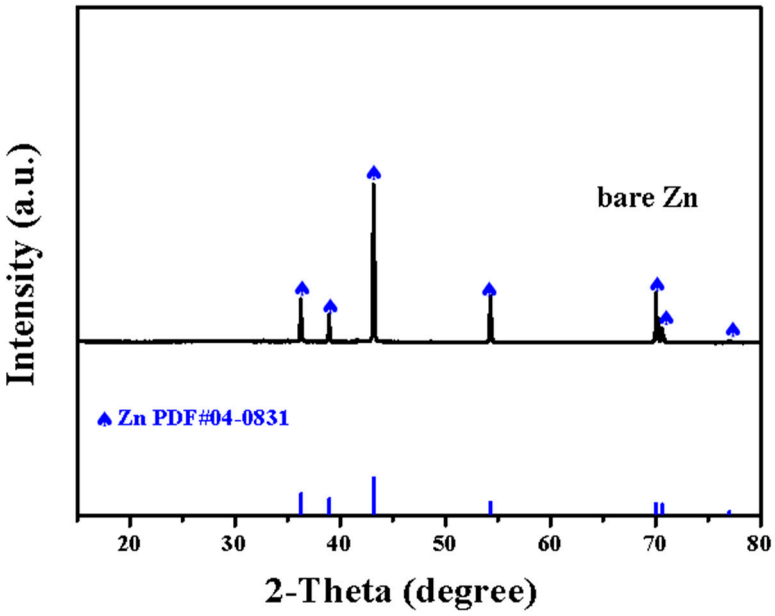

Figure S6. X-ray diffraction pattern of a bare Zn anode.

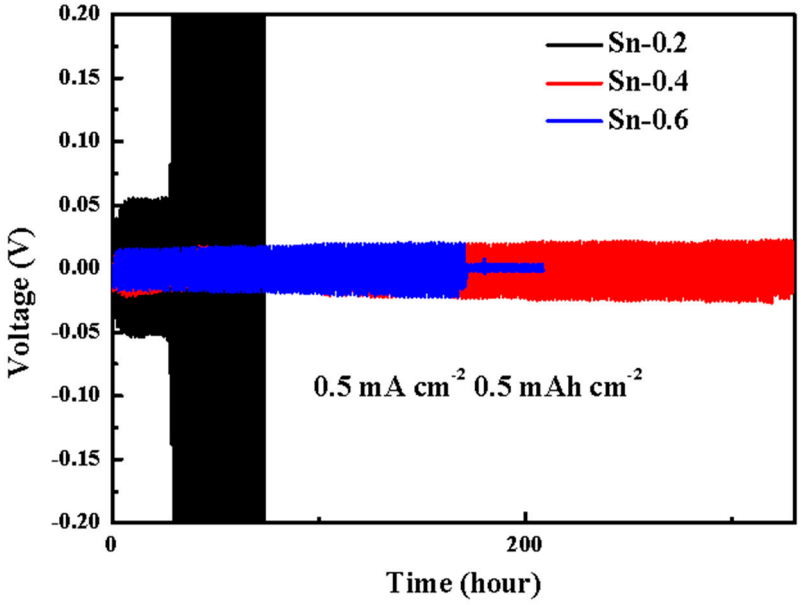

Figure S7. Cycling performance of ZSN anodes prepared with different concentrations of $SnCl_4$ in symmetric cells at 1 mA cm^{-2} for 0.5 mAh cm^{-2}.

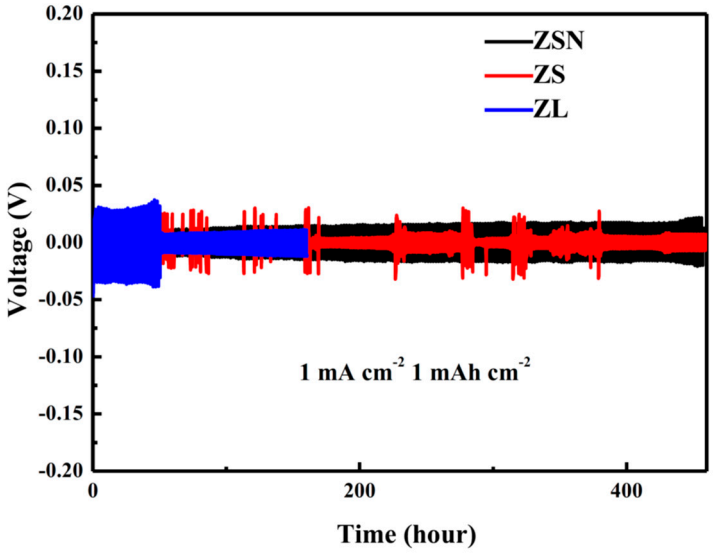

Figure S8. Comparison of the cycling performance of ZL, ZS, and ZSN anodes in symmetric cells at 1 mA cm^{-2} and 1 mAh cm^{-2}.

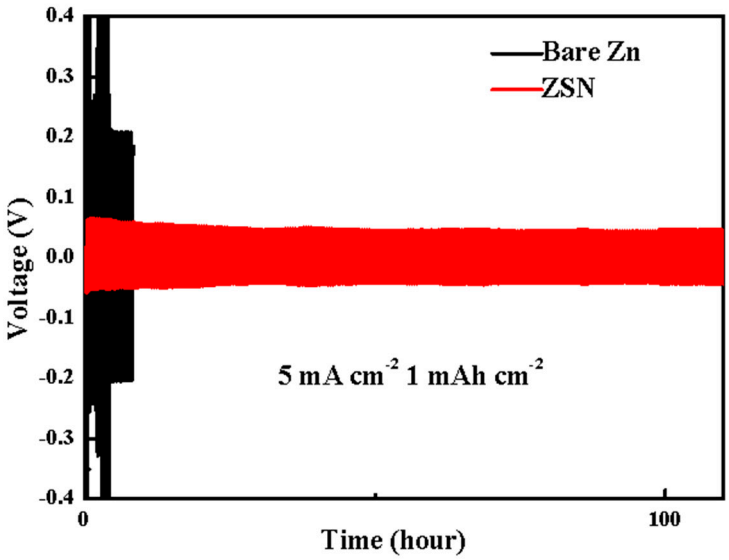

Figure S9. Cycling performance of bare Zn and ZSN anodes at 5 mA cm^{-2} and 1 mAh cm^{-2}.

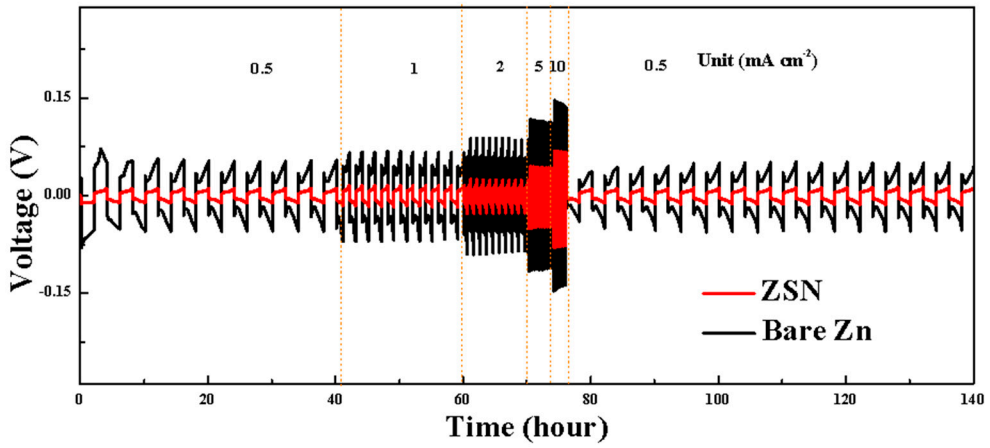

Figure S10. Rate performance of symmetric cells based on bare Zn and ZSN anodes at current densities from 0.5 to 10 mA cm^{-2}.

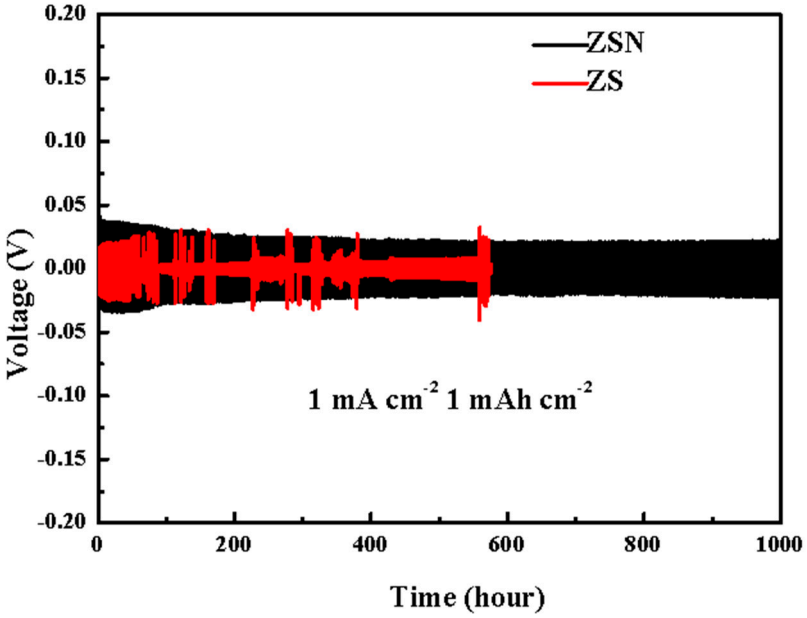

Figure S11. Cycling performance of ZS and ZSN anodes at 1 mA cm^{-2} for 1 mAh cm^{-2}.

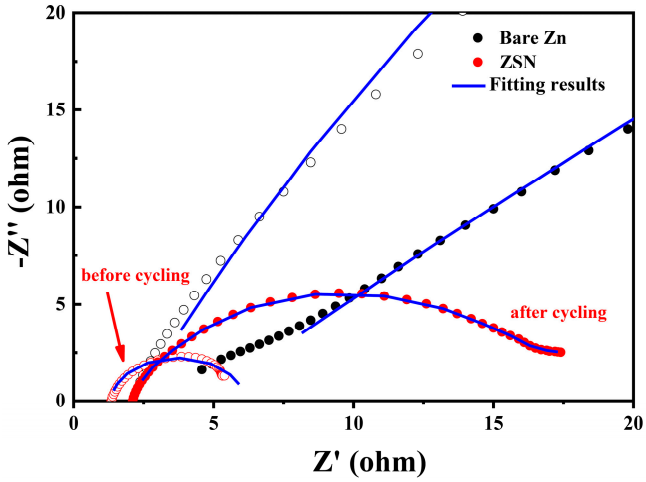

Figure S12. Impedance spectra of symmetric cells using ZSN and bare Zn electrodes before and after 50 cycles.

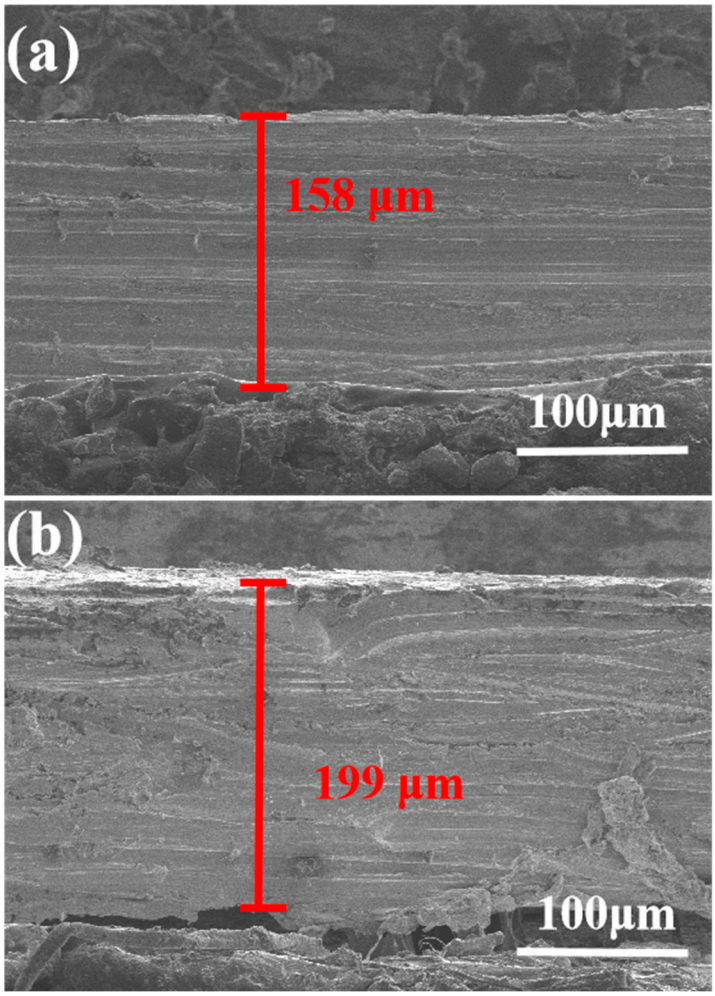

Figure S13. Cross-sectional SEM images of the bare Zn electrode (a) before cycling and (b) after 50 cycles at 1.0 mA cm^{-2} with a capacity of 1 mA h cm^{-2} in a symmetric cell.

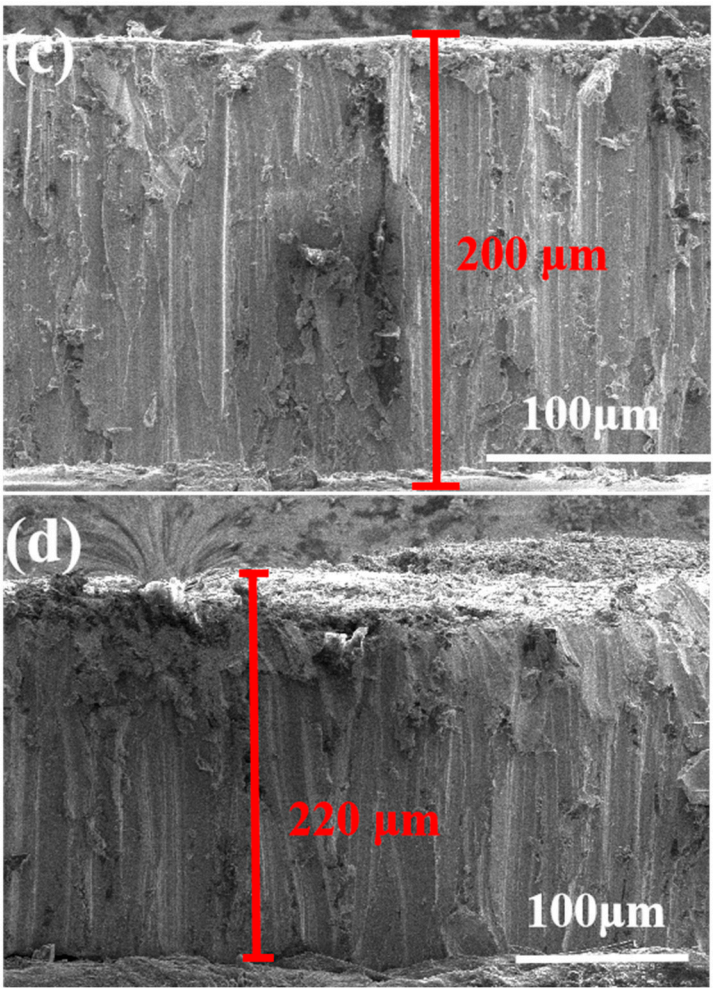

Figure S14. (a, b) Cross-sectional SEM images of the ZSN electrode after 100 cycles at 1 mA cm^{-2} and 1 mAh cm^{-2}.

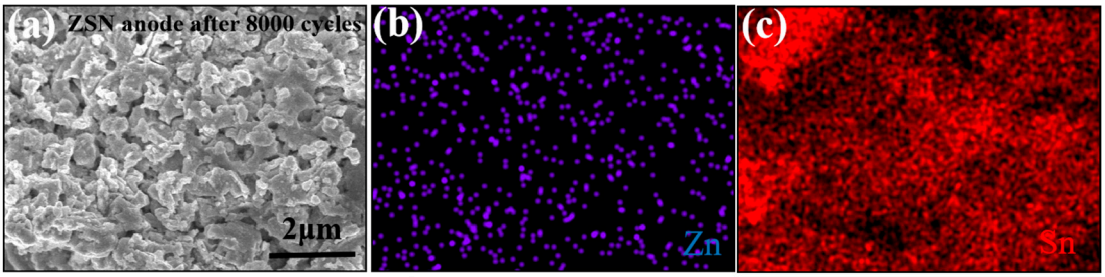

Figure S15. SEM and EDS images of the cycled anode in the ZSN ‖ AC system.

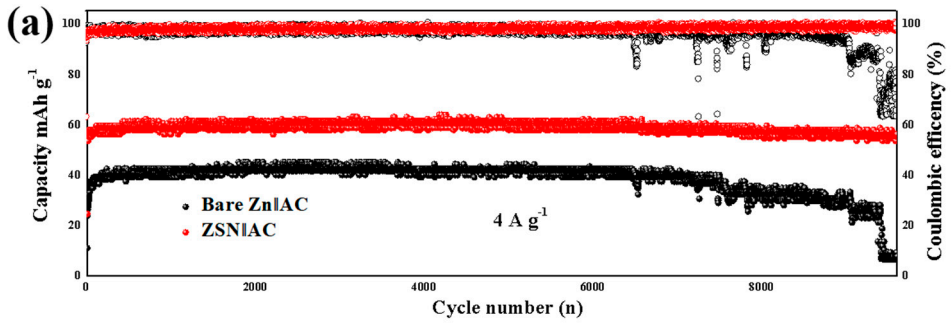

Figure S16. (a) Long-term cycling capability curves at 4 A g^{-1} of Zn ‖ AC and ZSN ‖ AC.

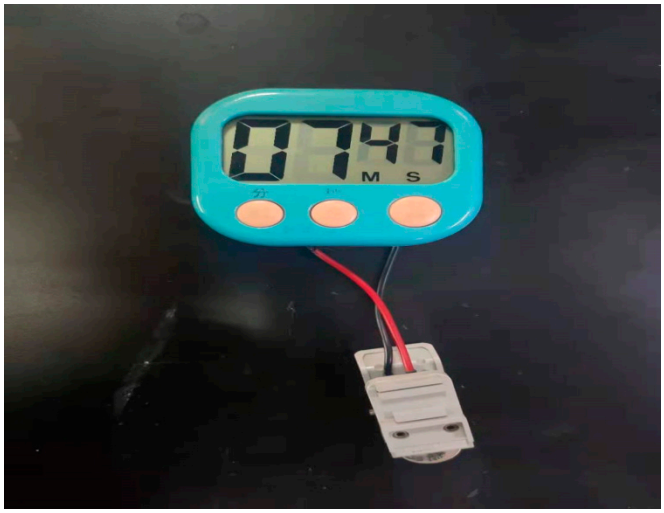

Figure S17. Photographic image of a normally working electronic chronograph driven by the ZSN‖MVO cells.

Table S1. Electrochemical performance of Zn stripping/plating of recently Zn/Zn symmetrical cells.

Materials	**Current density (mA cm^{-2})**	**Specific capacity (mAh cm^{-2})**	**Overpotential (mV)**	**Reference**
3D ZSN	**1**	**1**	**20**	**This work**
PPy-coated Zn	1	1	25	*Mater. Today Energy* **2020**, 17, 100443.
3D porous Zn	1	1	40	*J. Power Sources* **2020**, 479, 228808.
Zn@hydrogen-substitutedgraphdiyne	1	0.1	62	*Adv. Mater*. **2020**, 2001755.
Zn-AgNWs	2	2	36	*ACS Appl. Mater. Interfaces* **2022**, 14, 9097−9105.
Zn@Bi-pvdf	0.5	1	100	*J. Colloid Interf. Sci* **2022**, 617, 422–429.
FLG2@Zn	1	1	55	*J. Alloys Compd* **2022**, 617, 422–429.
Zn@ZrP	0.5	1	45.8	*Chem. Eng. J* **2022**, 432, 134227.

Table S2. Comparison of the cycling performance of ZSN ‖ AC supercapacitor with some recently reported representative AC capacitors.

Sample	R1	R2	CPE	W
ZSN‖AC	0.2687	10.89	$4.8048*10^{-4}$	145.5
Zn‖AC	1.931	15.02	$7.4348*10^{-5}$	94.18
ZSN‖AC after 50 cycles	1.57	19.51	$1.1092*10^{-5}$	8.154
Zn‖AC after 50 cycles	2.292	37.31	$5.0957*10^{-5}$	61.92

Table S3. Comparison for the cycling performance of the ZSN ‖ AC supercapacitor with recently reported AC-based capacitors.

Materials	**Energy density (Wh Kg $^{-1}$)**	**Current density (A g $^{-1}$)**	**Electrolyte**	**Reference**
ZSN ‖ AC	**53.3**	**2**	2 M H_2SO_4	**This work**
Co_3N//AC	12.1	1	6.0 M KOH	*Nat. Commun.* **2016**, 7, 12647.
AC//NiCoN/NC	41.7	1	1 M KOH	*ACS Appl. Mater.* Interfaces **2022**, 14, 47517−47528
Mo_2N//AC	16.3	1	1 M H_2SO_4	*ACS Energy Lett*. **2017**, 2, 336−341.
AC//NiCoN/NC	37.1	1	1 M KOH	*Adv. Funct. Mater.* **2014**, 24, 2630−2637.
NCZF//KOH//AC	49.3	1	1 M KOH	*Energy Storage Mater.* **2020**, 17, 100429
AC‖rGO-SnCu/Zn	37.64	2	2 M H_2SO_4	*Appl. Surf. Sci.* **2023**, 613, 156129

Table S4. Cycling performance for the ZSN ‖ MVO battery compared with recently reported batteries using MVO cathodes.

Materials	**Capacity (mAh g^{-1})**	**Current density (A g^{-1})**	**Percentage Capacity retained (%)**	**Reference**
ZSN ‖ MVO	**201**	**2**	**95.4% after 470 cycles**	**This work**
AZ-Zn/MVO	250	1	45% after 500 cycles	*Chem. Eng. J.* **2023**, 462, 142270
MnVO@C	250	5	91% after 500 cycles	*Energy Environ. Sci.* **2021**, 14, 3954-3964
NFZP@Zn/MnO_2	94	0.8	70% after 500 cycles	*Energy Storage Mater.* **2022**, 47, 491–499.
AlN/Ag@Zn‖MVO	143	5	70% after 2000 cycles	*ACS Nano* **2023**, 17, 337−345.
MnV_2O_6 (MVO)	88	1	104% after 2000 cycles	*Small* **2021**, 17, 2008182.
Mn ‖ MnVO	80	5	86.7% after 200 cycles	*Nat. Commun.* **2021**, 12, 6991.